Effect of second-order coupling on photon-pair statistics in waveguide structures

Yehonatan Gilead and Yaron Silberberg

Effect of Second-Order Coupling On Photon-Pair Statistics In Waveguide Structures

Yehonatan Gilead* and Yaron Silberberg

Department of Physics of Complex Systems, Weizmann Institute of Science, Rehovot 76100, Israel

(Dated: October 17, 2017)

We investigate a quasi-one-dimensional periodic array of coupled waveguides, with one extended and one bound dimension, incorporating both first- and second-order coupling. We study the evolution of optical fields in this system, and measure quantum correlations when path-entangled photon pairs are launched into them. We observe a surprisingly large and nontrivial effect of second-order coupling on these correlations - while quantum correlations are symmetric when only first-order coupling is present, the introduction of next-nearest-neighbor coupling often breaks the symmetry to reflections.

I. INTRODUCTION

In recent years, arrays of evanescently coupled optical waveguides have provided a fertile ground for experiments simulating condensed matter systems with optics, due to the analogy of the light field in a waveguide array and the electronic wavefunction on a lattice. One-dimensional arrays have been used to study quantum walks [1–4], Bloch oscillations [5, 6], Anderson localization [7, 8], and topological effects in quasi-crystals [9, 10]. More recently, the advent of femtosecond-laser writing [11, 12] has enabled the fabrication of 2-dimensional arrays, which have been used to examine 2D quantum walks [13], photonic graphene [14], transport properties of other two-dimensional structures [15, 16], and other effects [17, 18].

In addition, using light has granted the ability to investigate quantum interference, by inserting multi-photon states into these structures. In 1D structures, the aforementioned quantum walks show intriguing correlations between the output positions of the photons [19, 20]; other interesting results were found in arrays exhibiting Anderson localization [21–24]. In 2D, a few experiments were performed investigating quantum correlations (either using classical light to simulate the effects [25], or genuine quantum states [26, 27] showing nonclassical interference); these structures were, in general, limited to relatively few waveguides and displayed rather unstructured correlations.

In the works that examined 2D structures, both with classical and quantum light, the majority considered only nearest-neighbor, first-order coupling between waveguides; the exponential decay of the coupling strength with distance is assumed to make second order coupling negligible. Second-order coupling was theoretically addressed in zig-zag configuration [28], in order to simulate 1D lattices with second-order coupling; these were followed by experimental implementations as well [29]. Later on, photon-pair correlations were theoretically in-

vestigated in 1D lattices with second order coupling as well [30].

Here we investigate an ordered quasi-1D array of waveguides, which is extensive in one dimension and bound in the other. This is somewhat reminiscent of a two-leg ladder - a structure studied extensively in the condensed matter community [31], though usually with a focus on spin chains and not particle hopping transport; in general, most of these works also considered only nearest-neighbor coupling (though spin-one chains can be described as a two-leg ladder with diagonal coupling [32]). In more recent years, some attention has been given to particle transport in somewhat similar configurations [33, 34].

We investigate this system analytically in the context of light propagation, and present measurements with classical light demonstrating the predicted behavior. We then continue to calculate and measure quantum correlations of photon pairs propagating in this system, and show how the presence of second-order coupling can affect them - sometimes drastically.

II. EXPERIMENTAL SYSTEM

We perform these experiments in a system of evanescently coupled waveguides, fabricated in bulk glass utilizing the femtosecond-laser direct-write method [11, 12]. 300 fs-long laser pulses at 1 MHz repetition rate are used, with a central wavelength of 1041 nm. The pulses are slit-shaped [35] (in order to suppress polarization and angle dependence of the coupling), and then focused with a depth-corrected, 50x, NA=0.65 microscope objective into a Corning EAGLE2000 50 mm X 25 mm glass slide. The slide is translated at a speed of 40 mm per second along its long dimension, and the focus is placed approximately 125 μm below the glass surface - resulting in 50mm-long waveguides with a mode of approximately 9.5 μm full width at half maximum (FWHM).

A head-on schematic of the fabricated array is presented in Fig. 1(a). It is composed of two rows of waveguides; the vertical distance between the rows is 16μm, the horizontal distance between waveguides is 28μm, and the

---

* yehonatan.gilead@weizmann.ac.il
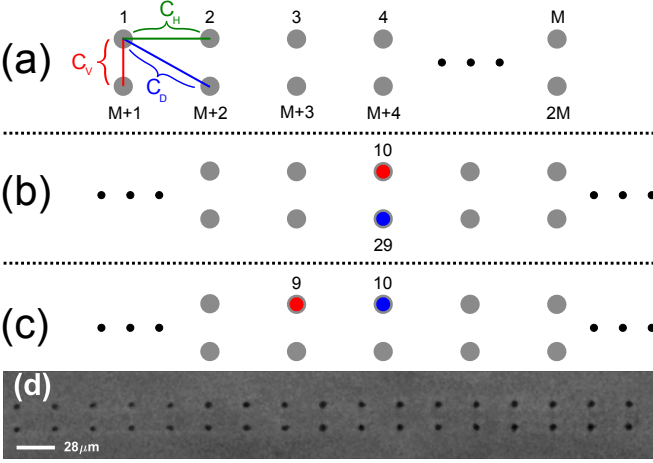
diagonal distance is therefore 32.25μm.

FIG. 1. (Color online) Schematic of the double-row waveguide array. The fabricated array extends over 25 waveguides horizontally, only part of which contain signal and are measured. (a) The site numbering for the measured waveguides begins in the top row, and continues on the bottom one. C_H, C_V and C_D are the horizontal, vertical and diagonal coupling constants, appropriately. (b) Input sites for the measurements with classical light. Two laser beams are coupled to vertically neighboring waveguides, with a controllable phase between them: $E_{10} = \frac{1}{\sqrt{2}}, E_{29} = e^{i\phi}\frac{1}{\sqrt{2}}$ (for these experiments, measurements were taken of M=19 waveguides in each row). (c) Input sites for the measurements with quantum light. Two photons are inserted in a superposition of being either in one waveguide on the top row, or its horizontal neighbor, with a controllable phase between the possibilities: $\frac{1}{2}\left(a_9^{\dagger 2} + e^{i\phi}a_{10}^{\dagger 2}\right)|0\rangle$ (for these experiments, measurements were taken of M=18 in each row). (d) Image of the glass slide facet, showing a cross section of a ladder array. This image has been processed to improve contrast, reduce the effect of noise, and correct for uneven lighting.

III. CLASSICAL LIGHT PROPAGATION

General analytical solutions to systems such as this have been previously shown in [36]. As this is a specialization of the general case presented there, the governing dynamics can be greatly simplified. With vertical, horizontal and diagonal coupling present, the propagation equation of the electric field amplitude is:

$$i\frac{\partial}{\partial z}A(z)_{h,v} = \beta A(z)_{h,v} + C_V A(z)_{h,v'} + C_H[A(z)_{h-1,v}+ \\ + A(z)_{h+1,v}] + C_D[A(z)_{h-1,v'} + A(z)_{h+1,v'}] \quad (1)$$

where A is the field amplitude, h is the index along the horizontal, long dimension, and v, v' are the two indices along the short, vertical dimension. β is the propagation constant in a single waveguide, C_V is the vertical

coupling constant between rows, C_H is the horizontal coupling constant inside a row, and C_D is the diagonal coupling constant. With some substitutions and implicit z-dependance, this equation can be expressed as (see appendix A for further detail):

$$i\frac{\partial}{\partial z}A_h^{(+)} = \beta^{(+)}A_h^{(+)} + C^{(+)}\cdot(A_{h-1}^{(+)} + A_{h+1}^{(+)}) \quad (2)$$

$$i\frac{\partial}{\partial z}A_h^{(-)} = \beta^{(-)}A_h^{(-)} + C^{(-)}\cdot(A_{h-1}^{(-)} + A_{h+1}^{(-)}) \quad (3)$$

With $A_h^{(+)} \equiv A_{h,u} + A_{h,d}$, $A_h^{(-)} \equiv A_{h,u} - A_{h,d}$, $\beta^{(+)} \equiv \beta + C_V$, $\beta^{(-)} \equiv \beta - C_V$, $C^{(+)} \equiv C_H + C_D$, $C^{(-)} \equiv C_H - C_D$, and u, d signifying the 'up' and 'down' rows. These equations are identical to an ordered 1D array, leading upon propagation to a pattern known as discrete diffraction [3]. This brings us to the conclusion that this system supports two general modes, a symmetric and an anti-symmetric one (as relating to the upper/lower row - for clarity we shall refer to them as the y-symmetric and y-anti-symmetric modes), each behaving identically to a 1D array with different effective propagation and coupling constants.

Specifically, one can show (appendix A) that the output from a single excited waveguide N on the top row will be:

$$A_{h,u}(z) = \frac{i^{h-N}}{2}\cdot[J_{h-N}(2zC^{(+)}) + e^{-2izC_V}J_{h-N}(2zC^{(-)})]$$
$$A_{h,d}(z) = \frac{i^{h-N}}{2}\cdot[J_{h-N}(2zC^{(+)}) - e^{-2izC_V}J_{h-N}(2zC^{(-)})]$$
$$(4)$$

For no diagonal coupling, $C^{(+)} = C^{(-)} = C_H$ and we get

$$A_{h,u}(z) = \frac{i^{h-N}}{2}\cdot J_{h-N}(2zC_H)(1 + e^{-2izC_V})$$
$$A_{h,d}(z) = \frac{i^{h-N}}{2}\cdot J_{h-N}(2zC_H)(1 - e^{-2izC_V}) \quad (5)$$

which is simply the 1D discrete diffraction pattern in each row, with power shifting between rows over propagation (see Fig. 2(a)). In reality, though, diagonal coupling is present; in our experiment, it was measured to be $C_D = 7.5 \pm 1.1$ m^{-1}, compared to the horizontal $C_H = 67.4 \pm 2.0$ m^{-1}. The vertical coupling C_V was not directly measured, but instead multiple arrays with different vertical distances were fabricated to find an equal-power setting. It is estimated to be approximately $C_V \simeq 580 \pm 60$ m^{-1}, with the large variance due to the short distance and lack of reliable calibration for vertically oriented arrays. In any case, as can be seen from Eq. (4), only the phase induced by this coupling is material to the results, and not its absolute value.
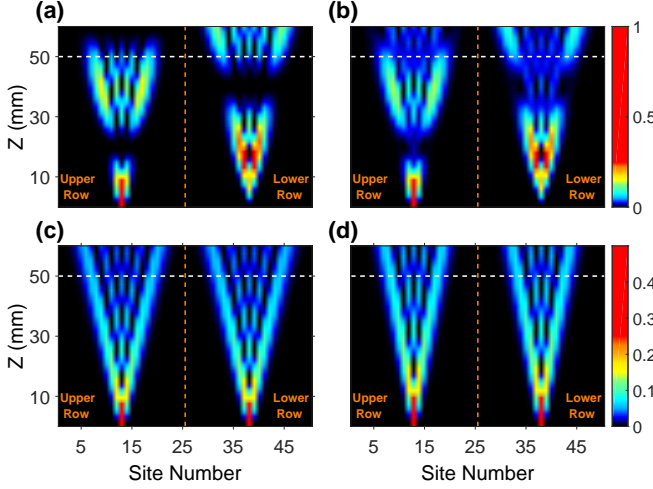
FIG. 2. (Color online) Simulations of intensity propagation of classical light in a double-row lattice. Following the numbering convention, the lower site numbers represent the upper row, and the higher ones represent the lower row, separated by the dashed, orange line. Note the color scales, which are saturated at higher values to allow details to be visible at later propagation distances. (a) Intensity along propagation when a single site on the upper row is initially excited, in a lattice with diagonal coupling turned *off*. The dashed white line is located such that the total power in the upper and lower rows are equal ($Z = \frac{n\pi}{4C_V}$, with n an odd integer. In this case, n =5, as C_V in these simulations is lower than the one in the experiment in order to maintain clarity in the graph). All measurements were taken at such a location. (b) Same as (a), with diagonal coupling turned *on*. Changes are evident, but are relatively small. (c,d) Intensity along propagation with diagonal coupling turned on, and the y-symmetric ($E_{10} = \frac{1}{\sqrt{2}}, E_{29} = \frac{1}{\sqrt{2}}$)(c) and y-anti-symmetric ($E_{10} = \frac{1}{\sqrt{2}}, E_{29} = \frac{-1}{\sqrt{2}}$)(d) modes excited. In either case, both rows experience the same discrete diffraction pattern, with a different effective coupling constant for either excitation mode.

The measured diagonal coupling is significantly smaller than expected from distance alone (calculated to be $\simeq 31.2$ m^{-1} from previously performed calibrations, assuming similar behaviour to that of horizontally coupled waveguides), possibly due to a masking effect similar to that observed for next-nearest-neighbor coupling in 1D lattices [37].

When diagonal coupling is introduced at this strength, the intensity output pattern from a single excited waveguide changes, to a degree qualitatively similar to that of the ratio $\frac{C_D}{C_H}$ (see Fig. 2(b), 3(a)). If the y-symmetric or y-anti-symmetric mode is directly excited, the output in each row becomes identical:
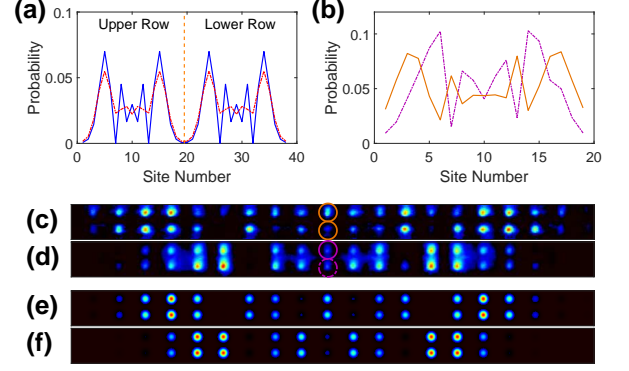

FIG. 3. (Color online) Output intensity distribution at an equal-power location (the white dashed line in Fig. 2). (a) Simulation of the intensity distribution at the output when site 10 is excited, at an equal-power location. When diagonal coupling is turned on (red, dashed line) and off (blue, solid line) power distribution changes, but not significantly. (b) Measured intensity distribution at the output, summed over both rows, when the y-symmetric (solid, orange line) and y-anti-symmetric (dashed, purple line) modes are excited. (c-f) CCD Images (c-d) and simulated images (e-f) of the power distribution at the output of the array, when the y-symmetric (c,e) and y-anti-symmetric (d,f) modes are excited. The circles mark the input waveguides.

$$A_{h,u}(z) = A_{h,d}(z) = A_{h,v}^{sym} = \frac{i^{h-N}}{2} \cdot J_{h-N}(2zC^{(+)}) \quad (6)$$

$$A_{h,v}^{asym} = \frac{i^{h-N}}{2} \cdot J_{h-N}(2zC^{(-)}) \quad (7)$$

For these excitations, the total power within each row remains constant, and both rows exhibit the same 1D discrete diffraction pattern - but with different effective coupling constants for the y-symmetric and y-anti-symmetric cases (see Fig. 2 (c,d)). Fig. 3(b-d) shows measured results of the output distribution when the y-symmetric and y-anti-symmetric modes are excited - the stronger effective coupling for the y-symmetric mode is clearly visible.

Surprisingly, regardless of whether the diagonal coupling is turned on or off, the eigenmodes of this system remain unchanged. Some intuition into this can be gained when one realizes that a change in the value of either the propagation constant β or the coupling constants $C^{(+)}$ and $C^{(-)}$ (or, in the case of no diagonal coupling or 1D, C_H) simply leads to a change in eigenvalues of the eigenmodes (appendix C). If we note the kth eigenmode of the 1D system as $\vec{V}^{(k)} = \sum_{m=1}^{M} V_m^{(k)}$ (with M being the number of sites in a row), the y-symmetric (y-anti-symmetric) eigenmodes of the 2D system will be $\vec{V}_u^{(k)} \pm \vec{V}_d^{(k)}$ whether the diagonal coupling is present or not - but with different eigenvalues in each case. This, in turn will lead to a change in the band structure of the system, as each mode will have a shifted energy.
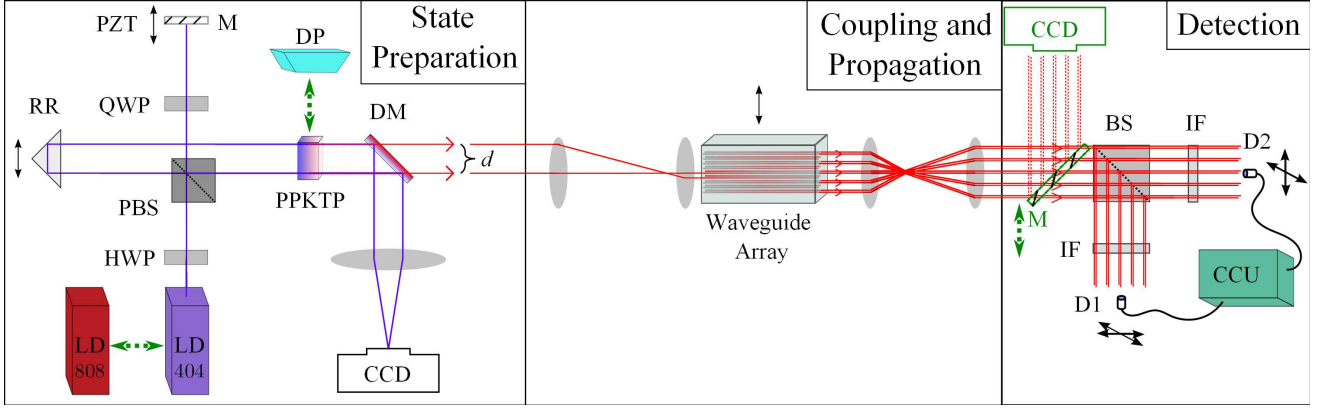
FIG. 4. (Color online) Experimental setup. LD - Laser Diode, HWP - Half-wave plate, PBS - Polarizing beam splitter, QWP - Quarter-wave plate, M - Mirror, RR - Retroreflector, PZT - Piezoelectric transducer, PPKTP - Nonlinear crystal, DP - Dove prism, DM - Dichroic mirror, CCD - Camera, BS - Beam splitter, IF - Interference filters, D1/2 - Fibre input facets, CCU - Coincidence counting unit. The elements in green frames (or marked by green arrows) are those inserted (or replaced) for the experiment using classical light.

IV. PROPAGATION OF ENTANGLED PHOTON PAIRS

So far, we have seen that the presence of weak diagonal coupling has no effect on the system's eigenmodes, and relatively little effect on the output power distribution from a single input (for the propagation distance considered here). Discernable differences are induced only when particular, multiple-site modes are intentionally excited. Considering this, one might ask - what effect will weak diagonal coupling have on correlations of photon pairs propagating through the structure?

To answer this question, we quantify these correlations with the photon-number correlation function (or correlation matrix) [19] $\Gamma_{q,r} = \langle a_q^\dagger a_r^\dagger a_r a_q \rangle$, where $a_q^\dagger$ is the creation operator for a photon in site number q. This matrix corresponds to the probability of detecting one photon in site q and the other in site r. Since we are dealing with a 2D structure, we will project the sites onto 1D to allow for ease of display of these matrices (following the convention in Fig. 1(a)) for a 2×18 section of the waveguide array.

We consider photon pairs inserted into the system in a path-entangled state $\frac{1}{2} \left(a_9^{\dagger^2} + e^{i\phi} a_{10}^{\dagger^2} \right) |0\rangle$; this corresponds to a superposition of the photons being inserted into either of two neighboring sites in the center of the top row, with a controlled phase between those possibilities.

A. State Preparation and Measurements

The experimental setup is presented in Figure 4. For the experiment using quantum light, the pump is a 404nm, 250mW continuous-wave laser diode, which is split into two beams in a Michelson-type interferometer. One arm is reflected by a mirror and the other by a retroreflector, such that they both exit the interferometer parallel to each other but with a distance d between them. The mirror is placed on a piezoelectric transducer to provide sub-wavelength control of the path length difference between the two beams.

The two beams are focused onto a nonlinear crystal (NLC, a 15mm-long crystal of periodically poled potassium titanyl phosphate, PPKTP) where they undergo type I spontaneous parametric down-conversion (SPDC), producing collinear, degenerate photon pairs. The pump beams are deflected by a dichroic mirror, and interfered on a CCD camera to produce a fringe pattern, from which the path length difference between the beams is measured. The SPDC beams are imaged onto the array's input facet, which couples them into the desired waveguide sites. The output from the array is split on a 50/50 non-polarizing beam splitter, before being imaged onto the input facets of 2 multimode fibres. Narrow band-pass interference filters (808±1.5 nm FWHM) are placed directly before the fibre input facets, to ensure indistinguishability between the detected photons by removing any non-degenerate pairs. The fibre input facets are placed on motorized stages, to allow scanning of the output of the array. The fibres are connected to single-photon counting modules, whose output is processed by a coincidence-counting unit implemented on an FPGA board. The time binning for coincidence was 7 ns.

The input state is verified by coupling the two beams to a 50/50 waveguide coupler, and observing oscillations in the coincidence rate between the two outputs, with a visibility of >80%.

Coincidences were measured between every possible pair of output waveguides, integrating over 30 seconds for each of the four input phases, for every one of the 1296 pairs in the 36-site lattice. The total coincidence rate, summed over all pairs at the lattice output, was approximately 20 KHz. Accidental coincidence counts
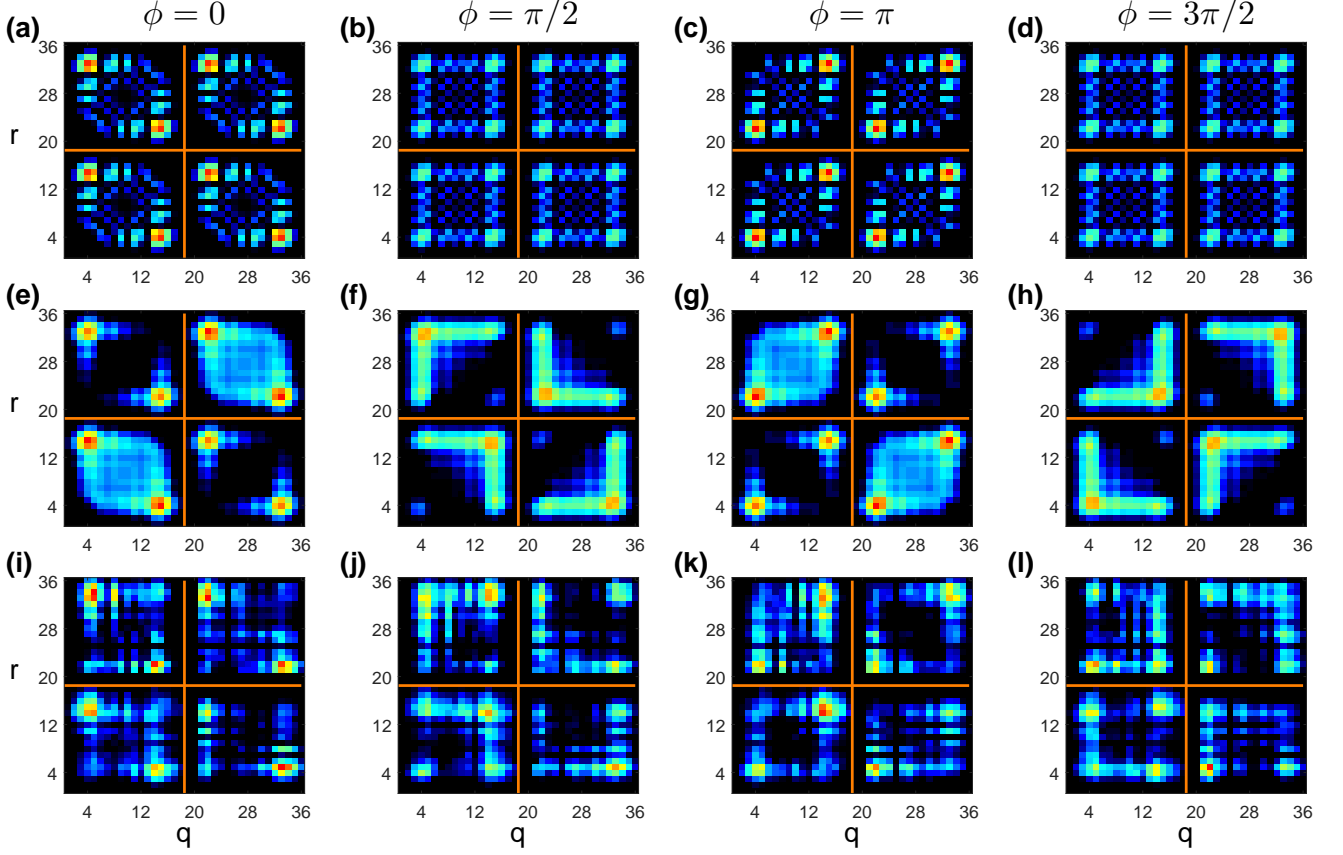
FIG. 5. (Color online) Correlation matrices $\Gamma_{q,r}$ for the double row lattice, for an input state of $\frac{1}{2}\left(a_9^{\dagger 2} + e^{i\phi}a_{10}^{\dagger 2}\right)|0\rangle$. The orange lines separate between the correlations of different rows; i.e., in each graph, the bottom-left quadrant represents the correlations inside the upper row, the upper-left/bottom-right represents the correlations between the different rows, and the top-right corner represents the correlations inside the bottom row (a-d) Simulated correlation matrices when diagonal coupling is turned *off*, for different phases ϕ. In this case, all quadrants display the same correlations, which are identical to those observed in a 1D lattice with similar input and only first-order coupling [19, 20]. (e-h) Same as (a-d), with diagonal coupling is turned *on*. While the correlations for the cases of $\phi = 0, \pi$ are relatively similar to those without diagonal coupling (same bunching and anti-bunching behavior), those for the cases of $\phi = \frac{\pi}{2}, \frac{3\pi}{2}$ show stark differences - the location of each photon is highly dependent on the location of the other, in a non-trivial manner. These dependencies are determined not only by their location within each row, but which row the are both in. (i-l) Experimentally measured, background-reduced correlation matrices, for a lattice with diagonal coupling as in (e-h). Although the results are quite noisy, the salient features are easily discerned. Contrast in these measurements may be reduced due to potential undesired overlap between the input beams and waveguides in the lower row.

were reduced in the results

For the experiment using classical light, the pump is replaced by a 808nm, 50mW laser diode, followed by appropriate polarization optics. The NLC is replaced by a dove prism to rotate the beams to vertical orientation. Additionally, the single-photon detection apparatus is replaced by a CCD camera.

B. Results

With no diagonal coupling, the correlations in each row and between rows are identical copies of the 1D correlations of the same input [19, 20] (Fig. 5(a-d)). When diagonal coupling is introduced, one might expect that the correlations would change in a modest degree, in a manner similar to that of the intensity distribution. For input phases $\phi = 0, \pi$, this is indeed the case - the correlations keep their bunching/anti-bunching characteristics, though some difference has been induced between the autocorrelation of rows and the cross-correlations between rows (Fig. 5(e,g,i,k)). In particular, photon pairs arriving at the center of the structure will do so in the same row for $\phi = 0$, and different rows for $\phi = \pi$.

On the other hand, for input phases $\phi = \pi/2, 3\pi/2$, the results are starkly different. Not only do they diverge from those of a system with no diagonal coupling, but they now show strong variations between correlations within a row and between them (Fig. 5(f,h,j,l)). *Without diagonal coupling, the location of one photon is totally*

independent of the location of the other (Fig. 5(b,d)); *with* diagonal coupling, this independence has been replaced by an intricate correlation, which is affected by both horizontal location and the row in which each photon ends up.

For example, when $\phi = \pi/2$, if one photon is in the center of the upper row (for example, site 9), the other will be on the right edge of either row (sites 15, 33), but if one is in the center of the bottom row (site 27), the other will be on the left side of either row (sites 4,22)). The contrast in these correlations is significant - much more than what one might expect, considering the relative weakness of the diagonal coupling and the small effect it had on single-particle output.

Perhaps the most glaring difference diagonal coupling causes in those phases is the disappearance of the symmetry to reflections along the horizontal axis between the input sites (i.e., left to right. For clarity, we will refer to this as *x-symmetry*). In the correlation matrices presented in Fig. 5, this reflection is implemented by rotating each individual quadrant by 180 degrees (as the rows do not mix in this transformation, the quadrants do not mix as well). This result is somewhat counterintuitive, as one may wonder how the addition of diagonal coupling (which itself has both x- and y-symmetry) manages to insert the new x-asymmetries visible at these phases.

Upon closer inspection, we realize that the correlation matrices at those phases should not a priori be x-symmetric, as the input state is x-asymmetric (as opposed to input states with $\phi = 0, \pi$, which are x-symmetric up to a global phase). In fact, the x-symmetric correlations in those phases for the case with no diagonal coupling are a result of an equivalence between the y-symmetric and y-anti-symmetric propagation modes introduced when diagonal coupling is turned off ($C^{(-)} = C^{(+)}$); this causes the correlations to degenerate to those of a 1D lattice with only first-order coupling (see appendix B).

Somewhat unexpectedly, such a lattice will *always* show x-symmetry in its correlations, even for x-*asymmetric* inputs - therefore, so will our ladder system with no diagonal coupling. We see from this that when considering first-order coupling alone, both these systems have an enforced x-symmetry in their correlations. Realizing the significant effect of second-order coupling on quantum correlations in our ladder system, we examined the effect of including second-order, next-nearest-neighbor couplings in a 1D lattice (previous works [30] have theoretically examined such a system, but only with input phases $\phi = 0, \pi$). Others have previously calculated the field amplitude at the output of such a 1D lattice [29]:

$$U_{q,m} = \sum_k i^{q-m-k} \cdot J_{q-m-2k}(2zC_H)J_k(2zC_{H2}) \quad (8)$$

where q is the output site index, m is the input site index, and C_{H2} is the next-nearest-neighbor coupling.

Applying it to Eq. (B5) (see appendix B) to calculate the correlation matrix $\Gamma_{q,r}$, we get an expression containing products of sums of elements, each with a different phase. From this we can surmise they will not be identical for all $\phi = \pm\phi_0$, and will thus also break the x-symmetry; numerical simulations of this system prove this is indeed the case (Fig. 6).
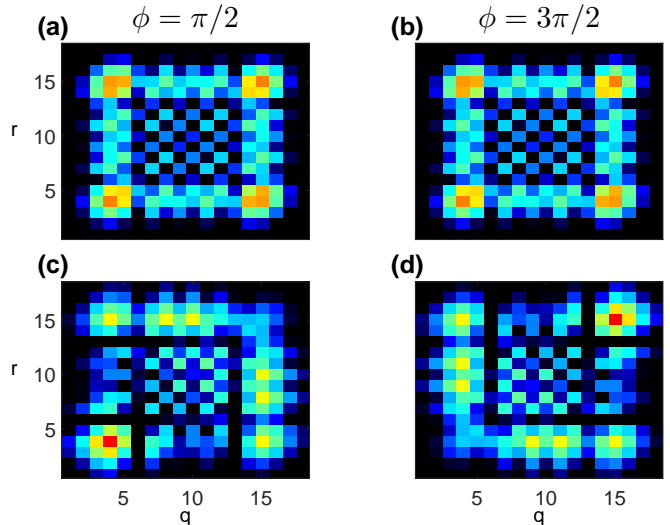

FIG. 6. (Color online) Simulated correlation matrices $\Gamma_{q,r}$ for a 1D lattice, for an input state of $\frac{1}{2}\left(a_9^{\dagger 2} + e^{i\phi}a_{10}^{\dagger 2}\right)|0\rangle$ (identical to that used in the experiment). (a-b) A 1D lattice with only nearest-neighbor coupling [19, 20]. For both phases $\phi = \frac{\pi}{2}, \frac{3\pi}{2}$, the correlations are identical and symmetric about the center of the array. (c-d) Same as (a-d), with second-order coupling present. Here, the correlations are no longer identical nor symmetric.

This shows that adding second-order, diagonal coupling to our ladder system, or second-order coupling to a 1D system, will relax the enforcement and remove the x-symmetry in correlations for these x-asymmetric input states. This, of course, is true for all such states ($\phi \neq 0, \pi$), and not just those measured in the experiment.

V. DISCUSSION

These results show that in general, the second-order coupling is often justifiably neglected, for experiments focusing on single-particle statistics. Even in our experimental system, which was designed to enhance the relative strength of this coupling (by implementing as short a vertical distance as feasible), it was found to be weaker than predicted - leading to a relatively small effect on propagation of single particles.

Despite this, we learn that when the propagation of photon pairs is examined, even weak coupling can lead to drastic changes in their correlations at the output.

These changes are shown to be present in both our experimental system and a 1D system with second-order coupling. Hence, we can surmise that when propagation of higher-order, multi-particle correlations are studied, one might also need to take into consideration higher-order coupling effects, which may not be significant for single-particle inputs.

In conclusion, we've studied a quasi-1D system of coupled waveguides with diagonal, second-order coupling, examining the prorogation of both classical and quantum light. We analytically solve the propagation equation, showing the existence of y-symmetric and y-antisymmetric modes, which we experimentally observe with classical light. For weak values of diagonal coupling, we observe the single-particle behavior to be rather similar to that of a system with no diagonal coupling.

We then proceed to predict and experimentally measure quantum correlations among photon pairs propagating in this structure. These show stark contrast with the case with no second-order coupling, even for weak values. These changes include the unveiling of an x-asymmetery which is hidden when second-order coupling is ignored - showing the sensitivity of photon-pair statistics to second-order coupling.

Appendix A: Analytic Expressions for Propagation Equations

We begin with the initial expression presented in the main text:

$$i\frac{\partial}{\partial z}A(z)_{h,v} = \beta A(z)_{h,v} + C_V A(z)_{h,v'} + C_H[A(z)_{h-1,v} + A(z)_{h+1,v}] + C_D[A(z)_{h-1,v'} + A(z)_{h+1,v'}] \quad (A1)$$

where A is the field amplitude, h is index along horizontal, long dimension, and v, v' are the two indices along the short, vertical dimension. β is the propagation constant in a single waveguide, C_V is the vertical coupling between rows, C_H is the horizontal coupling inside a row, and C_D is the diagonal coupling. To solve this, we will replace v's with u, d to signify the 'up' and 'down' row, and write the equations separately for each row:

$$i\frac{\partial}{\partial z}A_{h,u} = \beta A_{h,u} + C_V A_{h,d} + C_H(A_{h-1,u} + A_{h+1,u}) + C_D(A_{h-1,d} + A_{h+1,d}) \quad (A2)$$

$$i\frac{\partial}{\partial z}A_{h,d} = \beta A_{h,d} + C_V A_{h,u} + C_H(A_{h-1,d} + A_{h+1,d}) + C_D(A_{h-1,u} + A_{h+1,u}) \quad (A3)$$

where the z-dependence is implicit. We then re-form into the sum and difference of the two equations:

$$i\frac{\partial}{\partial z}(A_{h,u} + A_{h,d}) = (\beta + C_V)(A_{h,u} + A_{h,d}) + (C_H + C_D) \cdot [(A_{h-1,u} + A_{h-1,d}) + (A_{h+1,u} + A_{h+1,d})] \quad (A4)$$

$$i\frac{\partial}{\partial z}(A_{h,u} - A_{h,d}) = (\beta - C_V)(A_{h,u} - A_{h,d}) + (C_H - C_D) \cdot [(A_{h-1,u} - A_{h-1,d}) + (A_{h+1,u} - A_{h+1,d})] \quad (A5)$$

and then make the substitutions: $A_h^{(+)} \equiv A_{h,u} + A_{h,d}$, $A_h^{(-)} \equiv A_{h,u} - A_{h,d}$, $\beta^{(+)} \equiv \beta + C_V$, $\beta^{(-)} \equiv \beta - C_V$, $C^{(+)} \equiv C_H + C_D$, $C^{(-)} \equiv C_H - C_D$, yielding:

$$i\frac{\partial}{\partial z}A_h^{(+)} = \beta^{(+)}A_h^{(+)} + C^{(+)} \cdot (A_{h-1}^{(+)} + A_{h+1}^{(+)}) \quad (A6)$$

$$i\frac{\partial}{\partial z}A_h^{(-)} = \beta^{(-)}A_h^{(-)} + C^{(-)} \cdot (A_{h-1}^{(-)} + A_{h+1}^{(-)}) \quad (A7)$$

These equations are identical to the 1D array, leading upon propagation to a pattern known as discrete diffraction [3]. The solutions to these equations are therefore [38]:

$$A_h^{(+)}(z) = e^{i\beta^{(+)}z} \sum_{m=-\infty}^{\infty} i^{h-m} J_{h-m}(2zC^{(+)}) A_m^{(+)}(0) \implies \sum_{m=-\infty}^{\infty} i^{h-m} J_{h-m}(2zC^{(+)}) A_m^{(+)}(0) \tag{A8}$$

$$A_h^{(-)}(z) = e^{i\beta^{(-)}z} \cdot \sum_{m=-\infty}^{\infty} i^{h-m} J_{h-m}(2zC^{(-)}) A_m^{(-)}(0) \implies e^{-2izC_V} \sum_{m=-\infty}^{\infty} i^{h-m} J_{h-m}(2zC^{(-)}) A_m^{(-)}(0) \tag{A9}$$

where we shifted everything by a global phase factor $e^{-iz\beta^{(+)}}$. Substituting the original fields into this solution, we get:

$$A_{h,v}(z) = \frac{1}{2}(A_h^{(+)} + A_h^{(-)}) = \frac{1}{2} \sum_{m=-\infty}^{\infty} i^{h-m} \cdot \{A_{m,v}(0) \cdot [J_{h-m}(2zC^{(+)}) + e^{-2izC_V} J_{h-m}(2zC^{(-)})] +$$

$$+ A_{m,v'}(0) \cdot [J_{h-m}(2zC^{(+)}) - e^{-2izC_V} J_{h-m}(2zC^{(-)})]\} \tag{A10}$$

Appendix B: Correlation Symmetries to Horizontal Axis Reflections

We may now calculate the correlations arising from these results, for the input states and propagation distance used in the experiment. We can use the expression for the fields to obtain the unitary transformation matrix U [19]. For simplicity, we'll note $2zC^{(+)} \equiv x$ and $2zC^{(-)} \equiv x'$. For entangled photon pairs input in neighboring sites on the top row, in sites m and $m-1$ [initial state of $\frac{1}{2}\left(a_{m-1}^{\dagger 2} + e^{i\phi} a_m^{\dagger 2}\right)|0\rangle$], and at zC_V such that $e^{2izC_V} = i$, the relevant matrix elements are:

$$U_{q,u,m} = \frac{i^{q-m}}{2} \cdot [J_{q-m}(x) + iJ_{q-m}(x')] \tag{B1}$$

$$U_{q,d,m} = \frac{i^{q-m}}{2} \cdot [J_{q-m}(x) - iJ_{q-m}(x')] \tag{B2}$$

$$U_{q,u,m-1} = \frac{i \cdot i^{q-m}}{2} \cdot [J_{q-m+1}(x) + iJ_{q-m+1}(x')] \tag{B3}$$

$$U_{q,d,m-1} = \frac{i \cdot i^{q-m}}{2} \cdot [J_{q-m+1}(x) - iJ_{q-m+1}(x')] \tag{B4}$$

where q is the horizontal index and u, d are the vertical indices of the output site; $m, m-1$ are the horizontal input site indices. As an example, we will calculate the correlations only within the upper row (the same row as the input) Γ^{uu}, between horizontal sites q and r, with phase ϕ between the inputs:

$$\Gamma_{q,r}^{uu} = |U_{q,u,m}U_{r,u,m} + e^{i\phi}U_{q,u,m-1}U_{r,u,m-1}|^2 = \tag{B5}$$

$$\frac{1}{4}|i^{q-m} \cdot [J_{q-m}(x) + iJ_{q-m}(x')] \cdot i^{r-m} \cdot [J_{r-m}(x) + iJ_{r-m}(x')]$$

$$+ e^{i\phi}i \cdot i^{q-m} \cdot [J_{q-m+1}(x) + iJ_{q-m+1}(x')] \cdot i \cdot i^{r-m} \cdot [J_{r-m+1}(x) + iJ_{r-m+1}(x')]|^2$$

$$\implies$$

$$\Gamma_{q,r}^{uu} = \frac{1}{4}|i^{q+r-2m} \cdot [J_{q-m}(x) + iJ_{q-m}(x')] \cdot [J_{r-m}(x) + iJ_{r-m}(x')]$$

$$- e^{i\phi}i^{q+r-2m} \cdot [J_{q-m+1}(x) + iJ_{q-m+1}(x')] \cdot [J_{r-m+1}(x) + iJ_{r-m+1}(x')]|^2$$

$$\implies$$

$$\Gamma_{q,r}^{uu} = \frac{1}{4}|[J_{q-m}(x)J_{r-m}(x) - J_{q-m}(x')J_{r-m}(x')] + i \cdot [J_{q-m}(x)J_{r-m}(x') + J_{r-m}(x)J_{q-m}(x')]$$

$$- e^{i\phi} \cdot \{[J_{q-m+1}(x)J_{r-m+1}(x) - J_{q-m+1}(x')J_{r-m+1}(x')] + i \cdot [J_{q-m+1}(x)J_{r-m+1}(x') + J_{r-m+1}(x)J_{q-m+1}(x')]\}|^2$$

For no diagonal coupling, $x = x'$, so we get a simplified expression:

$$\Gamma_{q,r}^{uu} = \frac{1}{4} |[\cancel{J_{q-m}(x)J_{r-m}(x)} - \cancel{J_{q-m}(x)J_{r-m}(x)}] + i \cdot [J_{q-m}(x)J_{r-m}(x) + J_{r-m}(x)J_{q-m}(x)]$$
$$- e^{i\phi} \cdot \{[\cancel{J_{q-m+1}(x)J_{r-m+1}(x)} - \cancel{J_{q-m+1}(x)J_{r-m+1}(x)}] + i \cdot [J_{q-m+1}(x)J_{r-m+1}(x) + J_{r-m+1}(x)J_{q-m+1}(x)]\}|^2 \tag{B6}$$
$$\implies$$
$$\Gamma_{q,r}^{uu} = \frac{1}{4} |2 J_{q-m}(x)J_{r-m}(x) - e^{i\phi} \cdot 2 J_{q-m+1}(x)J_{r-m+1}(x)|^2 = |J_{q-m}(x)J_{r-m}(x) - e^{i\phi} \cdot J_{q-m+1}(x)J_{r-m+1}(x)|^2$$

This is identical to the result from the same input in a one-dimensional system with first-order coupling only [19]. Identical results are obtained for Γ^{ud}, Γ^{du},Γ^{dd} in this case.

When we examine reflections along the horizontal axis, we realize that changing the input phase from $\phi = \phi_0$ to $\phi = -\phi_0$ is equivalent to a reflection along the center between the input sites (since changing both leaves us in the same position). This shows that if the correlation matrix is in general identical for those two input phases, it must *also* be symmetric to reflections along the horizontal axis (x-symmetric); the converse is true as well.

As Bessel functions are real, for $\phi = \phi_0$, we will be adding a real number to a complex one and taking the absolute value squared. Another way to think of it is taking a horizontal vector in the complex plane, and adding another at angle $\phi = \phi_0$. Obviously, this shows how the correlations for $\phi = -\phi_0$ will be the same - we are implementing a reflection about the real axis in the complex plane, which will leave the total sum-vector length unaffected. The same will be true for a one-dimensional system without second order coupling, since it has the same correlation matrix.

Thus, any alteration that results in the correlation matrices for $\phi = \pm\phi_0$ no longer being identical will perforce cause the x-symmetry to vanish; this is the case with the addition of diagonal coupling to our ladder system, as well as with second-order coupling in a 1D system.

Appendix C: Equivalence of eigenmodes regardless of diagonal coupling

The Hamiltonian of the propagation equation for a 1D lattice is of the form:

$$\hat{H}_{1D} = \begin{pmatrix} \beta & C & 0 & 0 & \cdots \\ C & \beta & C & 0 & \cdots \\ 0 & C & \beta & C & \cdots \\ \vdots & \vdots & \vdots & \ddots & \vdots \\ 0 & 0 & \cdots & C & \beta \end{pmatrix} = \begin{pmatrix} \beta & 0 & 0 & 0 & \cdots \\ 0 & \beta & 0 & 0 & \cdots \\ 0 & 0 & \beta & 0 & \cdots \\ \vdots & \vdots & \vdots & \ddots & \vdots \\ 0 & 0 & \cdots & 0 & \beta \end{pmatrix} + \begin{pmatrix} 0 & C & 0 & 0 & \cdots \\ C & 0 & C & 0 & \cdots \\ 0 & C & 0 & C & \cdots \\ \vdots & \vdots & \vdots & \ddots & \vdots \\ 0 & 0 & \cdots & C & 0 \end{pmatrix}$$
$$= \beta \hat{I} + \hat{C} \tag{C1}$$

where the space is spanned by the number of sites on the array. If we take an eigenmode of this Hamiltonian, $\vec{V}^{(k)}$,

$$\hat{H}_{1D} \cdot \vec{V}^{(k)} = (\beta \hat{I} + \hat{C}) \cdot \vec{V}^{(k)} = \lambda_k \vec{V}^{(k)} \implies \hat{C} \cdot \vec{V}^{(k)} = (\lambda_k - \beta)\vec{V}^{(k)} \tag{C2}$$

showing that the eigenmodes of the matrix $\hat{C}$ are the eigenmodes of the hamiltonian, with shifted eigenvalues. Therefore, if we apply this hamiltonian with different parameters to the same eigenomodes, we will get:

$$\hat{H'}_{1D} \cdot \vec{V}^{(k)} = (\beta' \hat{I} + \hat{C}') \cdot \vec{V}^{(k)} = \left(\beta' \hat{I} + \frac{C'}{C}\hat{C}\right) \cdot \vec{V}^{(k)} = \left[\beta' + \frac{C'}{C}(\lambda_k - \beta)\right] \cdot \vec{V}^{(k)} \tag{C3}$$

showing that the eigenmodes are identical with a change in eigenvalues.

[1] S. Somekh, E. Garmire, A. Yariv, H. Garvin, and R. Hunsperger, Appl. Phys. Lett. **22**, 46 (1973).

[2] Y. Aharonov, L. Davidovich, and N. Zagury, Phys. Rev.

A **48**, 1687 (1993).

[3] F. Lederer, G. I. Stegeman, D. N. Christodoulides, G. Assanto, M. Segev, and Y. Silberberg, Physics Reports **463**, 1 (2008).

[4] H. B. Perets, Y. Lahini, F. Pozzi, M. Sorel, R. Morandotti, and Y. Silberberg, Physical Review Letters **100**, 170506 (2008).

[5] R. Morandotti, U. Peschel, J. S. Aitchison, H. S. Eisenberg, and Y. Silberberg, Phys. Rev. Lett. **83**, 4756 (1999).

[6] A. Szameit and S. Nolte, Journal of Physics B: Atomic, Molecular and Optical Physics **43**, 163001 (2010).

[7] Y. Lahini, A. Avidan, F. Pozzi, M. Sorel, R. Morandotti, D. Christodoulides, and Y. Silberberg, Physical Review Letters **100**, 013906 (2008).

[8] L. Martin, G. D. Giuseppe, A. Perez-Leija, R. Keil, F. Dreisow, M. Heinrich, S. Nolte, A. Szameit, A. F. Abouraddy, D. N. Christodoulides, and B. E. A. Saleh, Opt. Express, OE **19**, 13636 (2011).

[9] M. Verbin, O. Zilberberg, Y. E. Kraus, Y. Lahini, and Y. Silberberg, Physical Review Letters **110**, 076403 (2013).

[10] M. Verbin, O. Zilberberg, Y. Lahini, Y. E. Kraus, and Y. Silberberg, Physical Review B **91**, 064201 (2015).

[11] K. M. Davis, K. Miura, N. Sugimoto, and K. Hirao, Optics Letters **21**, 1729 (1996).

[12] S. Longhi, Laser & Photon. Rev. **3**, 243 (2009).

[13] T. Pertsch, U. Peschel, F. Lederer, J. Burghoff, M. Will, S. Nolte, and A. Tünnermann, Opt. Lett., OL **29**, 468 (2004).

[14] M. I. Molina and Y. S. Kivshar, Optics letters **35**, 2895 (2010); Y. Plotnik, M. C. Rechtsman, D. Song, M. Heinrich, J. M. Zeuner, S. Nolte, Y. Lumer, N. Malkova, J. Xu, A. Szameit, Z. Chen, and M. Segev, Nature Materials **13**, 57 (2013); M. C. Rechtsman, J. M. Zeuner, Y. Plotnik, Y. Lumer, D. Podolsky, F. Dreisow, S. Nolte, M. Segev, and A. Szameit, Nature **496**, 196 (2013).

[15] S. Mukherjee, A. Spracklen, D. Choudhury, N. Goldman, P. Öhberg, E. Andersson, and R. R. Thomson, Physical Review Letters **114**, 245504 (2015).

[16] S. Weimann, L. Morales-Inostroza, B. Real, C. Cantillano, A. Szameit, and R. A. Vicencio, Optics Letters **41**, 2414 (2016).

[17] R. Keil, C. Noh, A. Rai, S. Stützer, S. Nolte, D. G. Angelakis, and A. Szameit, Optica, OPTICA **2**, 454 (2015).

[18] F. Caruso, A. Crespi, A. G. Ciriolo, F. Sciarrino, and R. Osellame, Nature Communications **7**, 11682 (2016).

[19] Y. Bromberg, Y. Lahini, R. Morandotti, and Y. Silberberg, Physical Review Letters **102**, 253904 (2009).

[20] A. Peruzzo, M. Lobino, J. C. F. Matthews, N. Matsuda, A. Politi, K. Poulios, X.-Q. Zhou, Y. Lahini, N. Ismail, K. Wörhoff, Y. Bromberg, Y. Silberberg, M. G. Thompson, and J. L. OBrien, Science **329**, 1500 (2010).

[21] Y. Lahini, Y. Bromberg, D. N. Christodoulides, and Y. Silberberg, Phys. Rev. Lett. **105**, 163905 (2010).

[22] A. F. Abouraddy, G. Di Giuseppe, D. N. Christodoulides, and B. E. A. Saleh, Physical Review A **86**, 040302 (2012).

[23] A. Crespi, R. Osellame, R. Ramponi, D. J. Brod, E. F. Galvão, N. Spagnolo, C. Vitelli, E. Maiorino, P. Mataloni, and F. Sciarrino, Nature Photonics **7**, 545 (2013).

[24] Y. Gilead, M. Verbin, and Y. Silberberg, Phys. Rev. Lett. **115**, 133602 (2015).

[25] R. Keil, A. Szameit, F. Dreisow, M. Heinrich, S. Nolte, and A. Tünnermann, Physical Review A **81**, 023834 (2010).

[26] J. O. Owens, M. A. Broome, D. N. Biggerstaff, M. E. Goggin, A. Fedrizzi, T. Linjordet, M. Ams, G. D. Marshall, J. Twamley, M. J. Withford, and A. G. White, New Journal of Physics **13**, 075003 (2011).

[27] K. Poulios, R. Keil, D. Fry, J. D. A. Meinecke, J. C. F. Matthews, A. Politi, M. Lobino, M. Gräfe, M. Heinrich, S. Nolte, A. Szameit, and J. L. O'Brien, Phys. Rev. Lett. **112**, 143604 (2014).

[28] N. K. Efremidis and D. N. Christodoulides, Phys. Rev. E **65**, 056607 (2002).

[29] F. Dreisow, A. Szameit, M. Heinrich, T. Pertsch, S. Nolte, and A. Tünnermann, Optics letters **33**, 2689 (2008); A. Szameit, T. Pertsch, S. Nolte, A. Tünnermann, and F. Lederer, Physical Review A **77**, 043804 (2008); A. Szameit, R. Keil, F. Dreisow, M. Heinrich, T. Pertsch, S. Nolte, and A. Tünnermann, Optics letters **34**, 2838 (2009); G. Wang, J. P. Huang, and K. W. Yu, *ibid.* **35**, 1908 (2010); M. Golshani, A. R. Bahrampour, A. Langari, and A. Szameit, Physical Review A **87**, 033817 (2013).

[30] F. Qi, Z. G. Feng, Y. F. Wang, P. Xu, S. N. Zhu, and W. H. Zheng, Journal of Optics **16**, 125007 (2014).

[31] M. Troyer, H. Tsunetsugu, and T. M. Rice, Phys. Rev. B **53**, 251 (1996); E. Dagotto and T. M. Rice, Science **271**, 618 (1996); H.-H. Lin, L. Balents, and M. P. Fisher, Physical Review B **58**, 1794 (1998); M. Matsuda, K. Katsumata, R. S. Eccleston, S. Brehmer, and H.-J. Mikeska, Phys. Rev. B **62**, 8903 (2000).

[32] T. Giamarchi, *Quantum Physics in One Dimension* (Clarendon Press, New York, 2003) , p. 190.

[33] X. Li, E. Zhao, and W. Vincent Liu, Nature Communications **4**, 1523 (2013).

[34] W. Maimaiti, A. Andreanov, H. C. Park, O. Gendelman, and S. Flach, Phys. Rev. B **95**, 115135 (2017).

[35] M. Ams, G. D. Marshall, D. J. Spence, and M. J. Withford, Opt. Express, OE **13**, 5676 (2005).

[36] A. Szameit, T. Pertsch, F. Dreisow, S. Nolte, A. Tünnermann, U. Peschel, and F. Lederer, Phys. Rev. A **75**, 053814 (2007).

[37] R. Keil, B. Pressl, R. Heilmann, M. Gräfe, G. Weihs, and A. Szameit, Applied Physics Letters **107**, 241104 (2015).

[38] A. L. Jones, J. Opt. Soc. Am., JOSA **55**, 261 (1965).